catalysts

MDPI

Article

The Influence of the Gold Particle Size on the Catalytic Oxidation of 5-(Hydroxymethyl)furfural

Oliver Schade [1,2], Paolo Dolcet [1], Alexei Nefedov [3], Xiaohui Huang [4], Erisa Saraçi [2], Christof Wöll [3] and Jan-Dierk Grunwaldt [1,2,*]

[1] Institute for Chemical Technology and Polymer Chemistry, Karlsruhe Institute of Technology (KIT), D-76131 Karlsruhe, Germany; oliver.schade@kit.edu (O.S.); paolo.dolcet@kit.edu (P.D.)
[2] Institute of Catalysis Research and Technology, Karlsruhe Institute of Technology (KIT), D-76344 Eggenstein-Leopoldshafen, Germany; erisa.saraci@kit.edu
[3] Institute of Functional Interfaces, Karlsruhe Institute of Technology (KIT), D-76344 Eggenstein-Leopoldshafen, Germany; alexei.nefedov@kit.edu (A.N.); christof.woell@kit.edu (C.W.)
[4] Institute of Nanotechnology, Karlsruhe Institute of Technology (KIT), D-76344 Eggenstein-Leopoldshafen, Germany; xiaohui.huang@partner.kit.edu
* Correspondence: grunwaldt@kit.edu; Tel.: +49-721-608-42120

check for updates

Abstract: For the production of chemicals from biomass, new selective processes are required. The selective oxidation of 5-(Hydroxymethyl)furfural (HMF), a promising platform molecule in fine chemistry, to 2,5-furandicarboxylic acid (FDCA) is considered a promising approach and requires the oxidation of two functional groups. In this study, Au/ZrO_2 catalysts with different mean particle sizes were prepared by a chemical reduction method using tetrakis(hydroxymethyl)phosphonium chloride (THPC) and tested in HMF oxidation. The catalyst with the smallest mean particle size (2.1 nm) and the narrowest particle size distribution was highly active in the oxidation of the aldehyde moiety of HMF, but less active in alcohol oxidation. On the other hand, increased activity in FDCA synthesis up to 92% yield was observed over catalysts with a larger mean particle size (2.7 nm), which had a large fraction of small and some larger particles. A decreasing FDCA yield over the catalyst with the largest mean particle size (2.9 nm) indicates that the oxidation of both functional groups require different particle sizes and hint at the presence of an optimal particle size for both oxidation steps. The activity of Au particles seems to be influenced by surface steps and H bonding strength, the latter particularly in aldehyde oxidation. Therefore, the presence of both small and some larger Au particles seem to give catalysts with the highest catalytic activity.

1. Introduction

The depletion of fossil resources and the ever-growing demand for energy and chemical products drive the need to exploit renewable carbon sources such as biomass [1,2]. Inspired by current value chains that are based on a small number of platform chemicals like ethylene or propylene, the production of platform molecules through the partial fragmentation of biomass is one promising approach [3]. 5-(Hydroxymethyl)furfural (HMF) is considered one of the most versatile platform molecules that can be produced from carbohydrate biomass via dehydration [4–6]. More specifically, HMF is obtained from hexoses and can therefore also be produced from non-edible polymeric carbohydrates like cellulose [7]. As a platform molecule, HMF can undergo a variety of reactions like hydrogenation, [8] dehydrogenation [9], or hydrodeoxygenation [10]. Furthermore, the selective

oxidation of HMF has gained great interest in recent years. Selective oxidation of HMF can for example give 5-hydroxymethyl-2-furancarboxylic acid (HFCA) or 2,5-diformylfuran. One of the most important oxidation products is 2,5-furandicarboxylic acid (FDCA), [11,12] which is produced via the oxidation of both functional groups of HMF (Scheme 1). The structural similarity of FDCA to terephthalic acid led to its consideration as one of the twelve important molecules that can be produced from sugar-containing biomass feedstock [11,12]. Therefore, FDCA may be used in future bio-based polymers thus overcoming the need of petrochemical-based terephthalic acid [13,14]. Synthetic approaches for FDCA synthesis include stoichiometric oxidation reactions [15] as well as catalytic routes with mostly molecular oxygen. The latter range from bio- [16,17] to electro- [18–20] and metal catalysis. Current FDCA production is based on the homogeneously catalyzed AMOCO process, which is carried out in acetic acid solvent at 125 °C and 70 bar air in the presence of a Cu/Mn/Br catalyst [21]. In addition, heterogeneous metal catalysts have been applied in HMF oxidation. Especially supported noble metals like Pt [22–24] or Pd [25–27] are catalytically active in this reaction. Among others, supported gold-based catalysts show high activity in the oxidation of HMF with oxygen to FDCA [28–35]. For example, Au supported on CeO$_2$ nanoparticles allowed the production of FDCA in 96% yield after 5 h at 130 °C [28].
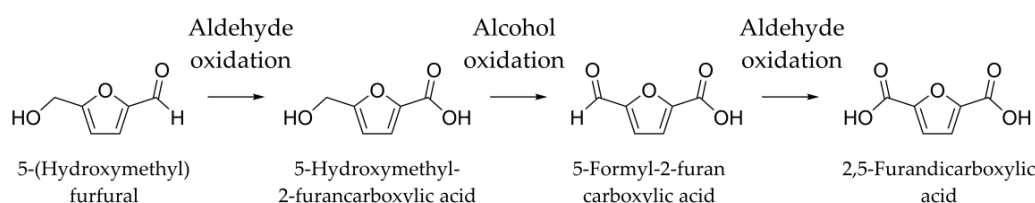
Scheme 1. Possible products and involved oxidation steps of 5-(Hydroxymethyl)furfural (HMF) oxidation over noble metal catalysts in alkaline solution.

Considering the chemical inertness of the bulk metal, gold has in early times been regarded to be catalytically inactive as well. However, small Au particles of few nanometers in size show catalytic activities in a variety of both gas and liquid phase reactions. Triggered by pioneering studies on gold-catalyzed oxidation of CO [36], gold catalysts have been used in a variety of oxidation reactions [37]. A special feature of gold catalysts is a strong dependence of catalytic activities on the gold particle size. For example, small particles of 2 nm in size were first found most active in the oxidation of CO [38] and propylene [39,40]. Later studies found that small clusters rather than nanoparticles are the catalytically active species [41], but such clusters may require high surface areas of the support material [42]. In contrast, slightly larger particles in the nanometer range (≈7 nm) are most active in alcohol oxidation [43,44].

Given that HMF bears two different functional groups, one alcohol and one aldehyde, and the strong influence of the Au particle size on the oxidation of different groups, an optimal Au particle size is needed to oxidize each group in high yields. In this study, we prepared gold catalysts of four different Au mean particle sizes (ranging from 2.1 to 2.9 nm) using a chemical reduction method with THPC. The catalysts were characterized and tested in the batch-wise oxidation of HMF, in which the influence of reaction temperature, amount of added base and air pressure were investigated.

2. Results

2.1. Catalyst Characterization

The starting gold colloids, prior to deposition on the ZrO$_2$ support, were analyzed by UV-Vis spectroscopy (Figure S1). The spectra showed very weak surface plasmon resonance (SPR) bands, indicating that the particle size of the Au nanoparticles is smaller than ≈3 nm. According to literature [38,45,46], below this value the SPR is strongly suppressed and surface scattering is the factor dominating the UV-Vis spectrum. The colloid with the expected larger size presents additionally a faint band centered at about 525 nm, indicating the possible presence of particles of up to 20 nm size.

The supported catalysts are labelled as AuZX, where Z represents the ZrO_2 support material and X represents the mean particle size by number based on scanning transmission electron microscopy (STEM, see text below and Figure 1). The metal loading (nominal loading: 2 wt.%) and the specific surface area of the four catalysts used in this study are listed in Table 1. Deposition of the gold colloids did not affect the specific surface area of the used ZrO_2 support material showing that the Au colloids or reductant did not block the pores of the support material. The support was added to the colloidal suspension to achieve a Au loading of 2 wt.%, however lower metal loadings show an incomplete deposition of the formed gold colloids on the support materials.
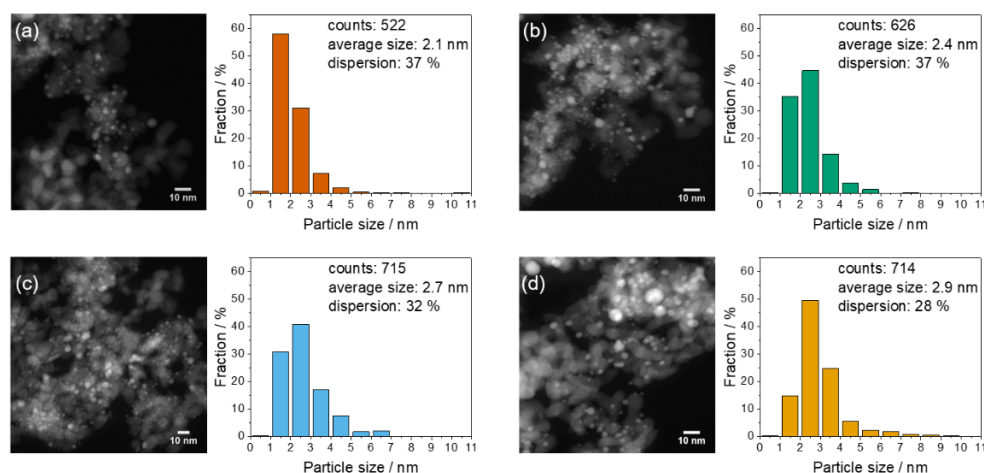

Figure 1. Representative STEM images and the corresponding particle size distributions by number of the four freshly prepared catalysts. The catalysts were labelled according to their mean particle sizes (**a**) AuZ2.1, (**b**) AuZ2.4, (**c**) AuZ2.7, and (**d**) AuZ2.9.

Table 1. Metal loading and specific surface area of the Au/ZrO_2 catalysts and the ZrO_2 support material.

Entry	Support/Catalyst	Au Loading/wt.%	Specific Surface Area/m^2 g^{-1}
1	ZrO_2	-	99
2	AuZ2.1	1.4	97
3	AuZ2.4	1.8	98
4	AuZ2.7	1.8	100
5	AuZ2.9	1.8	102

For none of the catalysts, were any reflections of gold observed in the powder X-ray diffraction (XRD) patterns (Figure S2). The absence of Au reflections is in good agreement with the Au loading and the expected particle sizes, which are below the detection limit of XRD [47]. In addition, similar diffraction patterns of the catalysts to the pure support material in all cases evidenced that ZrO_2 was stable in the colloidal suspension.

To gain insight into the particle sizes and size distributions of the catalysts, STEM images were recorded (Figure 1). AuZ2.1 (Figure 1a) shows a narrow particle size distribution with an average particle size of 2.1 nm at 37% dispersion. For this catalyst, 90% of all counted particles have a size of less than 3 nm with 58% of all particles being in the range of 1–2 nm. The average particle size is slightly larger than it was previously reported using this preparation procedure [43]. In contrast to the previous report, the increase in the particle size was not that pronounced for the four catalysts with average sizes of 2.4 nm, 2.7 nm, and 2.9 nm, respectively (Figure 1b–d). The increasing average particle size can be attributed to a broadening of the particle size distributions in all cases. This means, that for the catalysts b-d most particles are in the range of 2–3 nm (b: 45%, c: 41%, d: 50%), however, the fraction of large particles increases, which can both be seen in the representative TEM images as well as the particle size distributions (Figure 1). The difference in particle size distributions compared to literature might be explained by the fact that we used another support material and chose to characterize the final

supported catalysts. Possibly, larger particles were not adsorbed on the support material, which might also explain the slightly lower metal loading. Note that the trend in particle size prevails also when normalized to the surface atoms instead of the number of particles.

IR spectra were recorded for all the supported catalysts to investigate whether remains of the reducing agent THPC were still present in the catalysts (Figure 2). In contrast to the pure support material, all catalysts show two bands at 1130 cm^{-1} and 1052 cm^{-1}. In the basic solution (see details in the Experimental Section), bis(hydroxymethyl)phosphinic acid is formed from THPC [43]. Therefore, the bands can be assigned to the P = O (1130 cm^{-1}) and P-OH (1052 cm^{-1}) vibrations, respectively. This shows, that all catalysts still contained residues of THPC even after a thorough washing procedure.
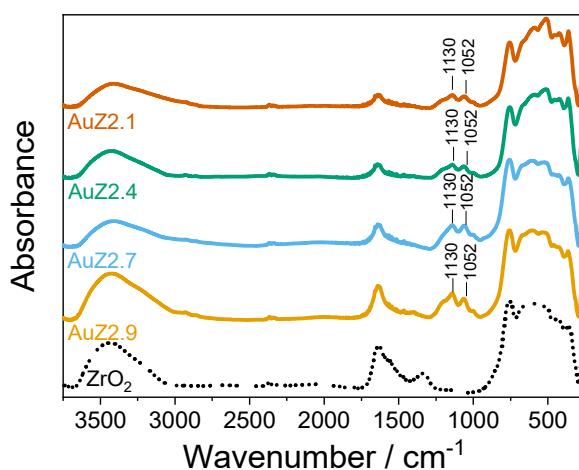

Figure 2. IR spectra of the supported as prepared catalysts and the pure ZrO$_2$ support (dotted line).

In order to quantify the surface contamination with remains of THPC, the catalysts were additionally characterized using X-ray photoelectron spectroscopy (XPS, Table 2, Figures S3 and S4). For all of them, the phosphorous content is indeed limited, and found in the range of 1–2 at%, with similar percentages also for gold. Only in the case of the sample with the largest average size the determined gold content is lower than 1 at% and therefore the P/Au ratio is four-fold that of the other samples. The samples contain also relevant amount of chlorine, originating both from the THPC and the gold precursor itself (tetrachloroauric acid). The latter is the most likely source, given the low amount of phosphorous present.

Table 2. Atomic percentages of the elements composing the surface of the samples, determined by XPS.

Entry	Catalyst	C/at%	O/at%	P/at%	Au/at%	Zr/at%	Cl/at%
1	AuZ2.1	49.4	33.1	1.4	1.0	6.9	8.2
2	AuZ2.4	42.9	38.9	0.9	1.0	8.4	7.9
3	AuZ2.7	43.0	37.6	1.8	1.6	7.4	8.6
4	AuZ2.9	35.5	38.3	1.6	0.4	12.0	11.0

The detailed analysis of the Au4f regions (Figure S4) showed that Au is mainly in metallic state (Au4f$_{7/2}$ ≈ 83.5 eV), while oxidized components (Au$^+$, Au4f$_{7/2}$ ≈ 86.7 eV) are limited to 2–5%. Although cationic Au species also correlated with HMF oxidation activity for Au/CeO$_2$ catalysts [48], their effect in this study is most likely not pronounced due to their low quantity, comparable among all the samples.

2.2. Catalytic Activity

The catalytic activity of all catalysts in HMF oxidation was studied under the same reaction conditions of 100 °C, 10 bar air pressure in the presence of four equivalents of NaOH (Table 3), based on

a thorough literature review (e.g., refs. [28,30,31,48,49]). A catalyst prepared by deposition-precipitation with a mean particle size of 3.7 nm (31% dispersion) was tested as a reference [50]. The generally lower product yields compared to Au/ZrO_2 prepared via deposition-precipitation (Table 3, entry 1) might be explained by the preparation procedure, since the reference sample was calcined (350 °C, 4 h) prior to testing while the samples discussed here were used as prepared to avoid particle growth. A possible influence could arise from the presence of the P and Cl contaminants, which might block some of the active sites of the gold nanoparticles. On the other hand, the trend in activity does not follow the variations seen for P and Cl contents since, e.g., AuZ2.9 with the highest relative contaminations has a productivity similar to that of AuZ2.4, which has the least amount of impurities. Hence, the difference in catalytic activity can be rationalized in terms of differences in noble metal particle size. Attributing differences in catalytic activity to the nanoparticle size rather than small Au clusters seems also reasonable, as the reaction is carried out in liquid phase and particles in the nanometer range are the ones active in alcohol oxidation [43,44]. Accordingly, nanoparticles rather than clusters will provide active sites. Furthermore, no correlation of the catalytic activity to the electronic structure of Au can be found. AuZ2.1 and AuZ2.9 are almost similar in terms of electronic structure based on XPS, but differ widely in their catalytic activity. This also underlines that the activity differences arise from the particle sizes.

Table 3. Catalyst screening of Au/ZrO_2 catalysts with different mean particle sizes in the oxidation of HMF. Reaction conditions: 100 °C, 10 bar air pressure, 4 equivalents of NaOH, 5 h reaction time, 1 mmol HMF in 10 mL H_2O, 98.5 mg catalyst.

Entry	Catalyst	HMF Conversion/%	Yield/%		C-Balance/%	Productivity [a]/mol_{FDCA} h^{-1} mol_{Au}^{-1}
			HFCA	FDCA		
1 [50]	Au/ZrO_2	100	0	75	75	19 (72)
2	AuZ2.1	100	9	16	25	5 (10)
3	AuZ2.4	100	0	35	35	8 (18)
4	AuZ2.7	100	0	43	43	10 (25)
5	AuZ2.9	100	1	30	31	7 (18)

a: Productivities normalized to surface Au atoms are given in brackets (mol_{FDCA} h^{-1} $mol_{Au,surface}^{-1}$).

Comparing the product yields under the same reaction conditions over the catalysts prepared by the colloidal method, although the particle size differences are rather small, a clear trend can be observed. AuZ2.1 gave the lowest carbon balance of 25% (Table 3, entry 2) with a FDCA yield of 16% and 9% yield of the intermediate HFCA. AuZ2.4 gave a higher FDCA yield of 35% and a maximum FDCA yield was observed over AuZ2.7, which produced FDCA in 43% yield. The differences in activity between AuZ2.1 and AuZ2.4 can be attributed to the particle size, since these catalysts have similar phosphorous and chloride content as well as fraction of cationic Au. No HFCA was produced over AuZ2.4 and AuZ2.7, indicating a high activity in the oxidation of the intermediate HFCA. AuZ2.9 with the largest mean particle size among the catalysts prepared by the colloidal method gave FDCA in a lower yield of 30% along with 1% of HFCA. The same trend is also reflected in the productivity, which normalizes the product yield to the reaction time and to the Au content thus eliminating any effect from the slightly different Au loadings. For AuZ2.7, the highest productivity rate of 10 mol_{FDCA} h^{-1} mol_{Au}^{-1} was obtained under these reaction conditions. Note, that the productivity was calculated based on the total amount of Au instead of the surface Au. Taking surface atoms into account in the calculation leads to a higher productivity because of the lower fraction of surface Au atoms. The trend persists, but the absolute values and relative differences between the catalysts increase (Table 3). AuZ2.4 and AuZ2.9 perform similarly when normalized to surface Au atoms with AuZ2.7 giving the highest productivity of 25 mol_{FDCA} h^{-1} $mol_{Au,surface}^{-1}$.

The influence of the reaction temperature on the oxidation of HMF is shown in Figure 3. Since HMF is unstable in basic aqueous solution and at high temperatures, [18] lowering the reaction temperature

results in a higher carbon balance. On the other hand, the oxidation of the hydroxymethyl group is the rate limiting step and often requires higher reaction temperatures [28]. Therefore, an optimal temperature as a compromise between reaction time and high yield has to be determined. As expected, a high carbon balance of above 80% was observed for all catalysts at 50 °C and HFCA was formed as the main product. This shows that all catalysts have a high activity in aldehyde oxidation, although there are slight differences. The highest carbon balance of 98% was observed for AuZ2.7, which yielded 73% of HFCA along with 25% of FDCA. This catalyst was active in alcohol oxidation even at a low temperature of 50 °C. Increasing the reaction temperature led to a reduction of the HFCA yield and the carbon balance for all catalysts. The HFCA yield decreased linearly over AuZ2.1 with increasing the temperature to 75 °C and FDCA yield just increased slightly from 1 to 16%. On the other hand, the selectivity shifted to FDCA at 75 °C for all catalysts except AuZ2.1, for which the selectivity switch occurred only at 100 °C, with a decreasing overall carbon balance. These results show that alcohol oxidation is the rate limiting step in this reaction, in line with literature [28] and is more pronounced for smaller Au particles (<2.4 nm). For the three catalysts with larger mean particle sizes, the highest FDCA yield of 55% was obtained at 75 °C (12 mol_{FDCA} h^{-1} mol_{Au}^{-1}). Also the surface-atom-normalized productivities increase with increasing particle size from 8, 29, 30 to 33 mol_{FDCA} h^{-1} $mol_{Au, surface}^{-1}$ over AuZ2.1, AuZ2.4, AuZ2.7, and AuZ2.9, respectively, showing superior activity of larger particles. Therefore, further catalytic experiments were carried out at this temperature, which was also chosen for AuZ2.1 in order to have comparable reaction conditions.
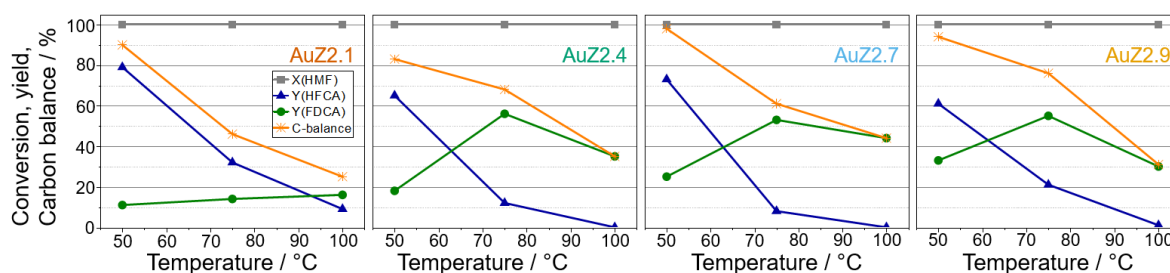

Figure 3. Influence of the reaction temperature on the product distribution in the oxidation of HMF over Au/ZrO$_2$ catalysts with different particle sizes. The AuZ2.1 catalyst with the smallest mean particle size is shown on the left side and the mean particle sizes increase towards the right side of the figure. Reaction conditions: 100 °C, 10 bar air pressure, HMF:NaOH 1:4, 5 h reaction time, 1 mmol HMF in 10 mL H$_2$O, 98.5 mg catalyst.

Reducing the amount of added base minimizes HMF degradation and enhances the sustainability of the reaction. However, the poor solubility of FDCA in water and the formation of a germinal diol as essential intermediate in the claimed reaction mechanism necessitate the use of a homogeneous base in most reactions [51]. Figure 4 shows the influence of NaOH addition on the product yields over all four catalysts. In all reactions that were conducted in the absence of base, a little amount of HMF was converted, showing some catalytic activity in the base-free oxidation of HMF. Under these conditions, the HMF conversion increased from 5 to 11% with increasing mean particle sizes. This indicates that the particle size of Au also affects HMF conversion. In the absence of base, some reactions gave HFCA in high selectivity. For example, HFCA was produced in 100% selectivity over AuZ2.4 at 7% HMF conversion. Increasing the amount of NaOH led to a linear increase in HFCA yield for all catalysts. At 1 equivalent of NaOH referred to HMF, HFCA was exclusively produced indicating that one hydroxide ion is required per oxidized functional group [51]. The highest HFCA yield of 93% was observed over AuZ2.1. Further increasing the amount of added base to two equivalents led to an increase in FDCA production, which was produced in the highest yield of 51% over AuZ2.7. Under these conditions, also AuZ2.1 produced some FDCA in 30% yield. Increasing the amount of added NaOH to 4 equivalents led to a further increase in FDCA production, which was produced in

a yield of around 55% over all catalysts other than AuZ2.1, which was the only catalyst that afforded less FDCA in 14% yield upon further increasing the amount of NaOH.
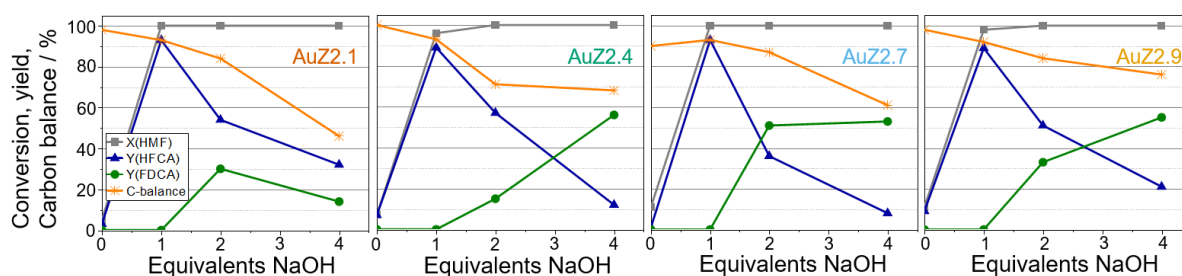

Figure 4. Influence of the amount of added NaOH on the product distribution in the oxidation of HMF over Au/ZrO$_2$ catalysts with different particle sizes. The AuZ2.1 catalyst with the smallest mean particle size is shown on the left side and the mean particle sizes increase toward the right side of the figure. Reaction conditions: 75 °C, 10 bar air pressure, HMF:NaOH 1:0/1/2/4, 5 h reaction time, 1 mmol HMF in 10 mL H$_2$O, 98.5 mg catalyst.

The influence of the air pressure was investigated as a last step and was performed at 75 °C in the presence of 4 equivalents of NaOH (Figure 5). As oxygen is consumed in the oxidation process, presumably by indirect participation in the mechanism, the yield of oxidation products should also increase with increasing pressure. A higher air pressure of 30 bar led to the exclusive production of FDCA for all catalysts, which was additionally produced in higher yields. Under these reaction conditions, FDCA was even produced in a high yield of 80% over AuZ2.1, which did not show a high activity in alcohol oxidation in the previous reactions. However, in line with the aforementioned studies, the FDCA yield over AuZ2.1 was the lowest under these conditions. Also at a higher air pressure of 30 bar, AuZ2.7 showed the highest activity in FDCA synthesis, which was produced in 92% yield at a productivity of 20 mol$_{FDCA}$ h^{-1} mol$_{Au}$. The differences in the productivity normalized to surface Au atoms becomes smaller here with the highest value of 53 mol$_{FDCA}$ h^{-1} mol$_{Au,surface}$$^{-1}$ for AuZ2.7 further underlining its superior activity. No leaching of Au (<1 ppm) was observed by means of ICP-OES except for AuZ2.9, which corresponded to 0.2% of the total Au content. Thus, the adsorption of pre-formed colloids resulted in strongly bound Au particles.
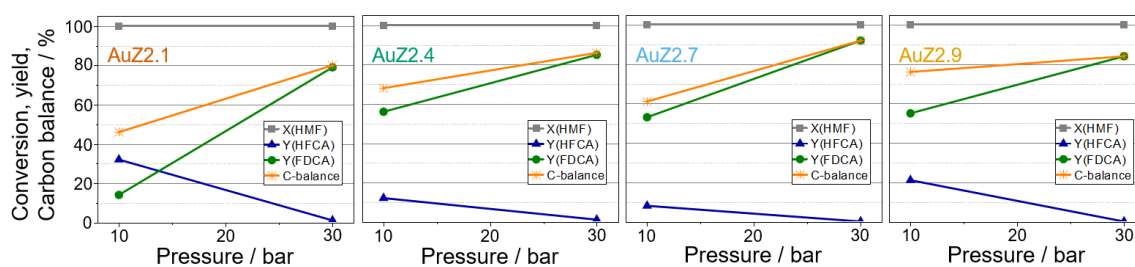

Figure 5. Influence of the air pressure on the product distribution in the oxidation of HMF over Au/ZrO$_2$ catalysts with different particle sizes. The AuZ2.1 catalyst with the smallest mean particle size is shown on the left side and the mean particle sizes increase towards the right side of the figure. Reaction conditions: 75 °C, HMF:NaOH 1: 4, 5 h reaction time, 1 mmol HMF in 10 mL H$_2$O, 98.5 mg catalyst.

3. Discussion

In this study, we investigated the particle size effect of small Au nanoparticles on the catalytic HMF oxidation by fine-tuning the size of Au particles. Mean particle sizes between 2.1 and 2.9 nm (286 atoms for 2.1 nm to 753 atoms for 2.9 nm) showed significant variations in activity and selectivity. The differences in the catalytic activity can most likely be attributed to different particle sizes, since other factors like e.g., the phosphorus or chloride contamination, did not show any clear

correlation. In addition, particles in the nanometer range rather than small clusters were most active in the oxidation of alcohols [44]. Recently, Megías-Sayago et al. [52] studied HMF oxidation over Au particles in the range of 4–40 nm supported on carbon. In contrast to our study, both the HMF conversion and HFCA yield were independent from the particle size at the larger particle sizes. Note that HMF conversion is 100% in most reactions due to its instability in alkaline solution. An increasing activity of smaller particles in alcohol oxidation of HMF was attributed to enhanced activity of such particles to reduce oxygen on Au(100), which are present to a larger extent on small particles. Consequently, oxygen is most probably activated on the Au particles in the present study as well, also considering the unlikely activation on the support. However, the used model only applies to particles with a size of more than 4 nm [52], which is larger than the mean sizes of particles used in this study also considering the small fraction of particles in this range for AuZ2.7 and AuZ2.9. Thus, the observed differences in catalytic activity can be attributed to the smaller particle sizes studied here.

The Au particle size is the most decisive factor influencing the catalytic activity of Au-based catalysts in liquid phase reactions, sometimes even more important than the support material [53]. In general, the effect of the support material in HMF oxidation is an active field of research and was attributed to the oxygen storage capacity [54], oxygen vacancies [48], or Brønsted acidity [55]. For ZrO_2, a low oxygen storage capacity was speculated to result in more active catalysts [54]. In addition, the support material affects the particle-support interactions. Carbon-supported Au catalysts might show different particle size dependencies, for example, intermediate particles were more active in the oxidation of ethylene glycol when supported on carbon instead of Al_2O_3, since smaller Au particles were located in micropores thus not accessible for the reactants [56]. The unlikely participation of the used ZrO_2 support material because of its low oxygen storage capacity combined with the fact that the same support material was chosen for all catalysts tested here further underline the difference in activity due to the particle size. This is also supported by no correlation between catalytic activity and Au electronic structure.

AuZ2.1 showed the narrowest particle size distribution and no larger particles were found in TEM analysis, therefore, its catalytic activity can be linked directly to the smallest gold particles. As AuZ2.1 showed the highest activity in HFCA production, i.e., aldehyde oxidation, and just a slight production of FDCA at 2 equivalents of NaOH, the smaller particles seem to be beneficial in the oxidation of the aldehyde but not the alcohol moiety of HMF when supported on ZrO_2. In contrast, AuZ2.9 also had a large fraction of small particles, however, with additional larger particles. Generally, catalysts with larger mean particle sizes were more active in FDCA synthesis, i.e., alcohol oxidation, in line with previous reports [43,57,58]. This might be due to the presence of surface steps, which are active in β-H removal [58], also considering that the reactions were carried out with excess NaOH [52]. This step is also an important part of the reaction mechanism in HMF oxidation, which probably follows a dehydrogenation mechanism [51,59]. During the reaction, the surface of Au particles gets covered by hydrogen [51,60]. Since the interaction between hydrogen and gold is stronger for smaller Au particles [61], active sites of AuZ2.1 may be blocked before being released after the reaction with oxygen, which might be the reason for FDCA production only with increasing air pressure. During the oxidation of the hydroxymethyl group, an aldehyde is formed in the first step [51]. Thus, the alcohol moiety of HMF is transformed into the aldehyde on larger particles, which in turn is converted on the smaller particles.

The instability of HMF in basic aqueous solution leads to humin formation, which lowers the carbon balance. Since, HFCA does not polymerize or decompose under these reaction conditions, it is therefore highly desirable to quickly convert HMF into HFCA before its thermal decomposition. This is particularly relevant with the alcohol oxidation being the rate-limiting step in HMF oxidation under such conditions. Therefore, the presence of a rather large fraction of small particles is beneficial for HMF oxidation, since HFCA is formed quickly. An increasing FDCA yield with the particle size up to AuZ2.7 shows that small but sufficiently large particles then oxidize the alcohol moiety and FDCA is formed.

4. Materials and Methods

4.1. Materials

Analytical grade chemicals were used without further purification: HMF, FDCA, THPC (Sigma-Aldrich, Darmstadt, Germany), HFCA, NaOH (Merck, Darmstadt, Germany), 2,5-diformylfuran, 5-formyl-2-furancarboxylic acid (TCI Chemicals, Eschborn, Germany), ZrO2 1/8″ pellets, $HAuCl_4 \cdot 3H_2O$ (Alfa Aesar, Karlsruhe, Germany), synthetic air (Air Liquide, Düsseldorf, Germany).

4.2. Catalyst Preparation

The catalysts were prepared by a modified chemical reduction method based on a previously established procedure [43]. In brief, gold colloids of different sizes were prepared by reducing alkaline solutions of $HAuCl_4$ with different molar ratios of the reducing agent THPC, which also acts as a stabilizing agent. After generation of the gold sol, powdered ZrO_2 was added to the acidified (pH = 2) colloidal suspension, stirred for 1 h and the resulting catalyst was separated by centrifugation and washed three times with water.

4.3. Catalyst Characterization

The starting colloids were analyzed, after 1:1 dilution with distilled water, by means of UV-Vis spectroscopy, using a Perkin Elmer Lambda 650 spectrometer.

X-ray diffraction (XRD) measurements of powder catalysts were recorded between diffraction angels 20° and 80° (step size 0.017°, 0.53 s acquisition time) using Cu K_α radiation (1.54600 Å) on a PANalytical (Malvern Panalytical, Kassel, Germany) X'Pert Pro instrument. In addition, rotating sample holders were used.

The gold content of the supported catalysts was determined by X-ray fluorescence (XRF, Bruker S4 Pioneer, Bruker, Billerica, MA, USA) and the concentration of gold in the reaction solutions was investigated using inductively coupled plasma optical emission spectrometry (ICP-OES, Agilent 720/725-ES, Agilent, Waldbronn, Germany).

The presence of organics on the supported catalysts was studied using infrared (IR) spectroscopy. For this purpose, the powder catalysts were pressed into a pellet with KBr and spectra were recorded in transmission mode (Agilent Varian 600-IR, Agilent, Waldbronn, Germany).

Specific surface areas of the catalysts and the corresponding support material were determined by N_2 physisorption according to the Brunauer–Emmet–Teller (BET) method. The catalysts were pretreated by heating to 300 °C for 2 h under reduced pressure, prior to adsorption (Rubotherm BELSORP-mini II, MicrotracBEL, Osaka, Japan).

Particle size distributions were determined based on transmission electron microscopy (TEM). For the measurements, a suspension of the catalysts in ethanol was deposited on holey carbon-coated gold grids. Scanning TEM (STEM) measurements were performed under high annular dark field (HAADF) using a Fischione (Fischione Instruments, Export, PA, USA) model 3000 HAADF-STEM detector on a FEI (Hillsboro, OR, USA) Titan 80–300 aberration corrected TEM instrument (300 kV). The particle size distribution was determined by fitting ellipsoid shapes to the noble metal particles using ImageJ software (National Institute of Health, Rockville, MD, USA). The dispersion of Au was calculated from the mean particle size under the assumption of spherical particles using tabulated values for the volume of Au atoms in bulk and the area of surface Au [62].

The XPS measurements were carried out under ultra-high vacuum with a base pressure in 10^{-10} mbar range. Core-level spectra were recorded under normal emission with a Scienta (Scienta Omicron, Uppsala, Sweden) R4000 electron analyzer using Al-Kα radiation (1486.6 eV). In addition to the survey XP spectra (Figure S3) the detailed C1s, O1s, P2p, Au4f, and Zr3d XP spectra were recorded. For the determination of the atomic percentage the CasaXPS software was used. In case of Au4f line the XP spectra were deconvoluted into two doublets corresponding to Au^0 and Au^{3+} states (Figure S4).

4.4. Selective Oxidation of HMF

Catalytic reactions were conducted in Teflon® inlets placed in home-built 52 mL autoclaves that were magnetically stirred. The appropriate amount of water was added to 5 mL of a 0.2 M HMF and the desired amount of NaOH was added as a 2.5 M solution to give a total volume of 10 mL. After the addition of the catalyst (calculated based on the nominal metal loading of 2 wt.%), the reactors were closed and the desired pressure was adjusted after purging the reactor three times with synthetic air. The stirring speed was set to the maximum value and the reactors were heated with heating sleeves controlled by a thermocouple inside the reaction mixture. The time at which the solution first reached the desired temperature was set as the starting point of the reaction (t = 0). The reactors were cooled to room temperature in an ice bath after the reactions followed by depressurizing and separating the catalyst via decantation. Samples of the liquid phase were taken before and after the reactions, filtered with a 0.45 µm Pall Teflon filter and diluted for HPLC analysis (HitachiPrimaide, Hitachi, Chiyoda, Tokyo, Japan, Bio-Rad Aminex HPX-87H column, solvent 5 mM H_2SO_4, temperature 50 °C, 50 bar).

5. Conclusions

Au particles with different sizes between 2.1 and 2.9 nm supported on ZrO_2 showed varying product distributions in HMF oxidation. While small particles were identified to be highly active in aldehyde oxidation, slightly larger particles favor alcohol oxidation. The differences in the catalytic activity can be attributed to the presence of surface steps on larger particles, which are important in alcohol oxidation as well as strongly bound H on smaller particles hindering further oxidation. These differences could only be revealed by the very fine-tuning of the Au particle size on ZrO_2. Therefore, an ideal HMF oxidation catalysts should have small and larger Au particles to generate a type of bifunctional catalysts of the same metal in order to achieve the highest activity in the oxidation of both functional groups of HMF.

References

1. Nikolau, B.J.; Perera, M.A.D.N.; Brachova, L.; Shanks, B. Platform biochemicals for a biorenewable chemical industry. *Plant J.* **2008**, *54*, 536–545. [CrossRef]
2. Henrich, E.; Dahmen, N.; Dinjus, E.; Sauer, J. The role of biomass in a future world without fossil fuels. *Chem. Ing. Tech.* **2015**, *87*, 1667–1685. [CrossRef]
3. Esposito, D.; Antonietti, M. Redefining biorefinery: The search for unconventional building blocks for materials. *Chem. Soc. Rev.* **2015**, *44*, 5821–5835. [CrossRef]

4.　van Putten, R.-J.; van der Waal, J.C.; de Jong, E.; Rasrendra, C.B.; Heeres, H.J.; de Vries, J.G. Hydroxymethylfurfural, A Versatile Platform Chemical Made from Renewable Resources. *Chem. Rev.* **2013**, *113*, 1499–1597. [CrossRef]

5.　Rosatella, A.A.; Simeonov, S.P.; Frade, R.F.M.; Afonso, C.A.M. 5-Hydroxymethylfurfural (HMF) as a building block platform: Biological properties, synthesis and synthetic applications. *Green Chem.* **2011**, *13*, 754–793. [CrossRef]

6.　Kuster, B.F.M. 5-Hydroxymethylfurfural (HMF). A Review Focussing on its Manufacture. *Starch-Stärke* **1990**, *42*, 314–321. [CrossRef]

7.　Steinbach, D.; Kruse, A.; Sauer, J. Pretreatment technologies of lignocellulosic biomass in water in view of furfural and 5-hydroxymethylfurfural production- A review. *Biomass Convers. Biorefin.* **2017**, *7*, 247–274. [CrossRef]

8.　Chatterjee, M.; Ishizaka, T.; Kawanami, H. Selective hydrogenation of 5-hydroxymethylfurfural to 2,5-bis-(hydroxymethyl)furan using Pt/MCM-41 in an aqueous medium: A simple approach. *Green Chem.* **2014**, *16*, 4734–4739. [CrossRef]

9.　Chatterjee, M.; Ishizaka, T.; Chatterjee, A.; Kawanami, H. Dehydrogenation of 5-hydroxymethylfurfural to diformylfuran in compressed carbon dioxide: An oxidant free approach. *Green Chem.* **2017**, *19*, 1315–1326. [CrossRef]

10.　Hengst, K.; Schubert, M.; Kleist, W.; Grunwaldt, J.-D. Hydrodeoxygenation of Lignocellulose-Derived Platform Molecules. In *Catalytic Hydrogenation for Biomass Valorization*; Rinaldi, R., Ed.; The Royal Society of Chemistry: Cambridge, UK, 2014; pp. 125–150.

11.　Werpy, T.; Petersen, G. *Top Value Added Chemicals from Biomass*; Natural Renewable Energy Laboratory: Golden, CO, USA, 2004.

12.　Bozell, J.J.; Petersen, G.R. Technology development for the production of biobased products from biorefinery carbohydrates-the US Department of Energy's "Top 10" revisited. *Green Chem.* **2010**, *12*, 539–554. [CrossRef]

13.　Sousa, A.F.; Vilela, C.; Fonseca, A.C.; Matos, M.; Freire, C.S.R.; Gruter, G.-J.M.; Coelho, J.F.J.; Silvestre, A.J.D. Biobased polyesters and other polymers from 2,5-furandicarboxylic acid: A tribute to furan excellency. *Polym. Chem.* **2015**, *6*, 5961–5983. [CrossRef]

14.　Zhang, D.; Dumont, M.-J. Advances in polymer precursors and bio-based polymers synthesized from 5-hydroxymethylfurfural. *J. Polym. Sci. Part A Polym. Chem.* **2017**, *55*, 1478–1492. [CrossRef]

15.　Miura, T.; Kakinuma, H.; Kawano, T.; Matsuhisa, H. Method for Producing Furan-2,5-dicarboxylic Acid. U.S. Patent 7,411,078, 12 August 2008.

16.　Krystof, M.; Pérez-Sánchez, M.; Domínguez de María, P. Lipase-Mediated Selective Oxidation of Furfural and 5-Hydroxymethylfurfural. *ChemSusChem* **2013**, *6*, 826–830. [CrossRef] [PubMed]

17.　Dijkman, W.P.; Groothuis, D.E.; Fraaije, M.W. Enzyme-Catalyzed Oxidation of 5-Hydroxymethylfurfural to Furan-2,5-dicarboxylic Acid. *Angew. Chem. Int. Ed.* **2014**, *53*, 6515–6518. [CrossRef] [PubMed]

18.　Vuyyuru, K.R.; Strasser, P. Oxidation of biomass derived 5-hydroxymethylfurfural using heterogeneous and electrochemical catalysis. *Catal. Today* **2012**, *195*, 144–154. [CrossRef]

19.　Barwe, S.; Weidner, J.; Cychy, S.; Morales, D.M.; Dieckhöfer, S.; Hiltrop, D.; Masa, J.; Muhler, M.; Schuhmann, W. Electrocatalytic Oxidation of 5-(Hydroxymethyl)furfural Using High-Surface-Area Nickel Boride. *Angew. Chem. Int. Ed.* **2018**, *57*, 11460–11464. [CrossRef]

20.　Taitt, B.J.; Nam, D.-H.; Choi, K.-S. A Comparative Study of Nickel, Cobalt, and Iron Oxyhydroxide Anodes for the Electrochemical Oxidation of 5-Hydroxymethylfurfural to 2,5-Furandicarboxylic Acid. *ACS Catal.* **2018**, *9*, 660–670. [CrossRef]

21.　Partenheimer, W.; Grushin, V.V. Synthesis of 2,5-Diformylfuran and Furan-2,5-Dicarboxylic Acid by Catalytic Air-Oxidation of 5-Hydroxymethylfurfural. Unexpectedly Selective Aerobic Oxidation of Benzyl Alcohol to Benzaldehyde with Metal=Bromide Catalysts. *Adv. Synth. Catal.* **2001**, *343*, 102–111. [CrossRef]

22.　Ait Rass, H.; Essayem, N.; Besson, M. Selective aqueous phase oxidation of 5-hydroxymethylfurfural to 2,5-furandicarboxylic acid over Pt/C catalysts: Influence of the base and effect of bismuth promotion. *Green Chem.* **2013**, *15*, 2240–2251. [CrossRef]

23.　Davis, S.E.; Houk, L.R.; Tamargo, E.C.; Datye, A.K.; Davis, R.J. Oxidation of 5-hydroxymethylfurfural over supported Pt, Pd and Au catalysts. *Catal. Today* **2011**, *160*, 55–60. [CrossRef]

24. Yu, H.; Kim, K.-A.; Kang, M.J.; Hwang, S.Y.; Cha, H.G. Carbon Support with Tunable Porosity Prepared by Carbonizing Chitosan for Catalytic Oxidation of 5-Hydroxylmethylfurfural. *ACS Sus. Chem. Eng.* **2018**, *7*, 3742–3748. [CrossRef]

25. Siyo, B.; Schneider, M.; Radnik, J.; Pohl, M.-M.; Langer, P.; Steinfeldt, N. Influence of support on the aerobic oxidation of HMF into FDCA over preformed Pd nanoparticle based materials. *Appl. Catal. A* **2014**, *478*, 107–116. [CrossRef]

26. Chen, C.; Li, X.; Wang, L.; Liang, T.; Wang, L.; Zhang, Y.; Zhang, J. Highly Porous Nitrogen- and Phosphorus-Codoped Graphene: An Outstanding Support for Pd Catalysts to Oxidize 5-Hydroxymethylfurfural into 2,5-Furandicarboxylic Acid. *ACS Sus. Chem. Eng.* **2017**, *5*, 1300–11306. [CrossRef]

27. Lei, D.; Yu, K.; Li, M.-R.; Wang, Y.; Wang, Q.; Liu, T.; Liu, P.; Lou, L.-L.; Wang, G.; Liu, S. Facet Effect of Single-Crystalline Pd Nanocrystals for Aerobic Oxidation of 5-Hydroxymethyl-2-furfural. *ACS Catal.* **2017**, *7*, 421–432. [CrossRef]

28. Casanova, O.; Iborra, S.; Corma, A. Biomass into Chemicals: Aerobic Oxidation of 5-Hydroxymethyl-2-furfural into 2,5-Furandicarboxylic Acid with Gold Nanoparticle Catalysts. *ChemSusChem* **2009**, *2*, 1138–1144. [CrossRef] [PubMed]

29. Gorbanev, Y.Y.; Klitgaard, S.K.; Woodley, J.M.; Christensen, C.H.; Riisager, A. Gold-Catalyzed Aerobic Oxidation of 5-Hydroxymethylfurfural in Water at Ambient Temperature. *ChemSusChem* **2009**, *2*, 672–675. [CrossRef] [PubMed]

30. Cai, J.; Ma, H.; Zhang, J.; Song, Q.; Du, Z.; Huang, Y.; Xu, J. Gold Nanoclusters Confined in a Supercage of Y Zeolite for Aerobic Oxidation of HMF under Mild Conditions. *Chem. Eur. J.* **2013**, *19*, 14215–14223. [CrossRef]

31. Miao, Z.; Zhang, Y.; Pan, X.; Wu, T.; Zhang, B.; Li, J.; Yi, T.; Zhang, Z.; Yang, X. Superior catalytic performance of $Ce_{1-x}Bi_xO_{2-\delta}$ solid solution and $Au/Ce_{1-x}Bi_xO_{2-\delta}$ for 5-hydroxymethylfurfural conversion in alkaline aqueous solution. *Catal. Sci. Technol.* **2015**, *5*, 1314–1322. [CrossRef]

32. Gupta, N.K.; Nishimura, S.; Takagaki, A.; Ebitani, K. Hydrotalcite-supported gold-nanoparticle-catalyzed highly efficient base-free aqueous oxidation of 5-hydroxymethylfurfural into 2,5-furandicarboxylic acid under atmospheric oxygen pressure. *Green Chem.* **2011**, *13*, 824–827. [CrossRef]

33. Gao, T.; Gao, T.; Fang, W.; Cao, Q. Base-free aerobic oxidation of 5-hydroxymethylfurfural to 2,5-furandicarboxylic acid in water by hydrotalcite-activated carbon composite supported gold catalyst. *Mol. Catal.* **2017**, *439*, 171–179. [CrossRef]

34. Masoud, N.; Donoeva, B.; de Jongh, P.E. Stability of gold nanocatalysts supported on mesoporous silica for the oxidation of 5-hydroxymethyl furfural to furan-2,5-dicarboxylic acid. *Appl. Catal. A* **2018**, *561*, 150–157. [CrossRef]

35. Schade, O.R.; Dannecker, P.-K.; Kalz, K.F.; Steinbach, D.; Meier, M.A.; Grunwaldt, J.-D. Direct Catalytic Route to Biomass-Derived 2,5-Furandicarboxylic Acid and Its Use as Monomer in a Multicomponent Polymerization. *ACS Omega* **2019**, *4*, 16972–16979. [CrossRef] [PubMed]

36. Haruta, M.; Kobayashi, T.; Sano, H.; Yamada, N. Novel Gold Catalysts for the Oxidation of Carbon Monoxide at a Temperature far Below 0 °C. *Chem. Lett.* **1987**, *16*, 405–408. [CrossRef]

37. Hashmi, A.S.K.; Hutchings, G.J. Gold Catalysis. *Angew. Chem. Int. Ed.* **2006**, *45*, 7896–7936. [CrossRef]

38. Grunwaldt, J.-D.; Kiener, C.; Wögerbauer, C.; Baiker, A. Preparation of Supported Gold Catalysts for Low-Temperature CO Oxidation via "Size-Controlled" Gold Colloids. *J. Catal.* **1999**, *181*, 223–232. [CrossRef]

39. Haruta, M.; Uphade, B.; Tsubota, S.; Miyamoto, A. Selective oxidation of propylene over gold deposited on titanium-based oxides. *Res. Chem. Intermed.* **1998**, *24*, 329–336. [CrossRef]

40. Haruta, M. When gold is not noble: Catalysis by nanoparticles. *Chem. Rec.* **2003**, *3*, 75–87. [CrossRef]

41. Herzing, A.A.; Kiely, C.J.; Carley, A.F.; Landon, P.; Hutchings, G.J. Identification of active gold nanoclusters on iron oxide supports for CO oxidation. *Science* **2008**, *321*, 1331–1335. [CrossRef]

42. Bogdanchikova, N.; Pestryakov, A.; Farias, M.; Diaz, J.A.; Avalos, M.; Navarrete, J. Formation of TEM-and XRD-undetectable gold clusters accompanying big gold particles on TiO_2–SiO_2 supports. *Solid State Sci.* **2008**, *10*, 908–914. [CrossRef]

43. Haider, P.; Kimmerle, B.; Krumeich, F.; Kleist, W.; Grunwaldt, J.-D.; Baiker, A. Gold-catalyzed aerobic oxidation of benzyl alcohol: Effect of gold particle size on activity and selectivity in different solvents. *Catal. Lett.* **2008**, *125*, 169–176. [CrossRef]

44. Adnan, R.H.; Andersson, G.G.; Polson, M.I.; Metha, G.F.; Golovko, V.B. Factors influencing the catalytic oxidation of benzyl alcohol using supported phosphine-capped gold nanoparticles. *Catal. Sci. Technol.* **2015**, *5*, 1323–1333. [CrossRef]

45. Tsunoyama, H.; Ichikuni, N.; Tsukuda, T. Microfluidic synthesis and catalytic application of PVP-stabilized, ~ 1 nm gold clusters. *Langmuir* **2008**, *24*, 11327–11330. [CrossRef] [PubMed]

46. Tofighi, G.; Lichtenberg, H.; Pesek, J.; Sheppard, T.L.; Wang, W.; Schöttner, L.; Rinke, G.; Dittmeyer, R.; Grunwaldt, J.-D. Continuous microfluidic synthesis of colloidal ultrasmall gold nanoparticles: In Situ study of the early reaction stages and application for catalysis. *React. Chem. Eng.* **2017**, *2*, 876–884. [CrossRef]

47. Sasirekha, N.; Sangeetha, P.; Chen, Y.-W. Bimetallic Au–Ag/CeO$_2$ catalysts for preferential oxidation of CO in hydrogen-rich stream: Effect of calcination temperature. *J. Phys. Chem. C* **2014**, *118*, 15226–15233. [CrossRef]

48. Li, Q.; Wang, H.; Tian, Z.; Weng, Y.; Wang, C.; Ma, J.; Zhu, C.; Li, W.; Liu, Q.; Ma, L. Selective oxidation of 5-hydroxymethylfurfural to 2,5-furandicarboxylic acid over Au/CeO$_2$ catalysts: The morphology effect of CeO$_2$. *Catal. Sci. Technol.* **2019**, *9*, 1570–1580. [CrossRef]

49. Albonetti, S.; Lolli, A.; Morandi, V.; Migliori, A.; Lucarelli, C.; Cavani, F. Conversion of 5-hydroxymethylfurfural to 2,5-furandicarboxylic acid over Au-based catalysts: Optimization of active phase and metal–support interaction. *Appl. Catal. B* **2015**, *163*, 520–530. [CrossRef]

50. Schade, O.R.; Kalz, K.F.; Neukum, D.; Kleist, W.; Grunwaldt, J.-D. Supported gold- and silver-based catalysts for the selective aerobic oxidation of 5-(hydroxymethyl)furfural to 2,5-furandicarboxylic acid and 5-hydroxymethyl-2-furancarboxylic acid. *Green Chem.* **2018**, *20*, 3530–3541. [CrossRef]

51. Davis, S.E.; Zope, B.N.; Davis, R.J. On the mechanism of selective oxidation of 5-hydroxymethylfurfural to 2,5-furandicarboxylic acid over supported Pt and Au catalysts. *Green Chem.* **2012**, *14*, 143–147. [CrossRef]

52. Megías-Sayago, C.; Lolli, A.; Bonincontro, D.; Penkova, A.; Albonetti, S.; Cavani, F.; Odriozola, J.A.; Ivanova, S. Effect of gold particles size over Au/C catalyst selectivity in HMF oxidation reaction. *ChemCatChem* **2020**, *12*, 1177–1183. [CrossRef]

53. Ishida, T.; Kinoshita, N.; Okatsu, H.; Akita, T.; Takei, T.; Haruta, M. Influence of the support and the size of gold clusters on catalytic activity for glucose oxidation. *Angew. Chem. Int. Ed.* **2008**, *47*, 9265–9268. [CrossRef]

54. Sahu, R.; Dhepe, P.L. Synthesis of 2,5-furandicarboxylic acid by the aerobic oxidation of 5-hydroxymethyl furfural over supported metal catalysts. *React. Kinet. Mech. Catal.* **2014**, *112*, 173–187. [CrossRef]

55. Megías-Sayago, C.; Chakarova, K.; Penkova, A.; Lolli, A.; Ivanova, S.; Albonetti, S.; Cavani, F.; Odriozola, J.A. Understanding the role of the acid sites in HMF oxidation to FDCA reaction over gold catalysts: Surface investigation on Ce$_x$Zr$_{1-x}$O$_2$ compounds. *ACS Catal.* **2018**, *8*, 11154–11164. [CrossRef]

56. Porta, F.; Prati, L.; Rossi, M.; Coluccia, S.; Martra, G. Metal sols as a useful tool for heterogeneous gold catalyst preparation: Reinvestigation of a liquid phase oxidation. *Catal. Today* **2000**, *61*, 165–172. [CrossRef]

57. Sun, K.-Q.; Luo, S.-W.; Xu, N.; Xu, B.-Q. Gold nano-size effect in Au/SiO$_2$ for selective ethanol oxidation in aqueous solution. *Catal. Lett.* **2008**, *124*, 238–242. [CrossRef]

58. Guan, Y.; Hensen, E.J. Ethanol dehydrogenation by gold catalysts: The effect of the gold particle size and the presence of oxygen. *Appl. Catal. A* **2009**, *361*, 49–56. [CrossRef]

59. Zope, B.N.; Hibbitts, D.D.; Neurock, M.; Davis, R.J. Reactivity of the Gold/Water Interface during Selective Oxidation Catalysis. *Science* **2010**, *330*, 74–78. [CrossRef]

60. Mondelli, C.; Ferri, D.; Grunwaldt, J.-D.; Krumeich, F.; Mangold, S.; Psaro, R.; Baiker, A. Combined liquid-phase ATR-IR and XAS study of the Bi-promotion in the aerobic oxidation of benzyl alcohol over Pd/Al$_2$O$_3$. *J. Catal.* **2007**, *252*, 77–87. [CrossRef]

61. Kartusch, C.; van Bokhoven, J.A. Hydrogenation over gold catalysts: The interaction of gold with hydrogen. *Gold Bull.* **2009**, *42*, 343–348. [CrossRef]

62. Bergeret, G.; Gallezot, P. Particle size and dispersion measurements. In *Handbook of Heterogeneous Catalysis*; Ertl, G., Knözinger, H., Schüth, F., Weitkamp, J., Eds.; Wiley-VCH: Weinheim, Germany, 2008; pp. 738–765.